Arch. Mech., **70**, 4, pp. 337–364, Warszawa 2018
SEVENTY YEARS OF THE ARCHIVES OF MECHANICS

NURBS-based optimization of natural frequencies for bidirectional functionally graded beams

N. I. KIM, T.A. HUYNH, Q. X. LIEU, J. LEE

Department of Architectural Engineering
Sejong University
209, Neungdong-ro, Gwangjin-gu
Seoul 05006, S. Korea
e-mails: kni8501@gmail.com, anhuynh@sju.ac.kr,
lieuxuanqui@gmail.com,
jhlee@sejong.ac.kr (corresponding author)

In this study, the nurbs-based isogeometric analysis is developed to optimize natural frequencies of bidirectional functionally graded (BFG) beams by tailoring their material distribution. One-dimensional Non-Uniform Rational B-Spline (NURBS) basis functions are utilized to construct the geometry of beam as well as approximate solutions, whereas the gradation of material property is represented by two-dimensional basis functions. To optimize the material composition, the spatial distribution of volume fractions of material constituents is defined using the higher order interpolation of volume fraction values that are specified at a finite number of control points. As an optimization algorithm, the differential evolution (DE) algorithm is employed to optimize the volume fraction distribution that maximizes each of the first three natural frequencies of BFG beams. A numerical analysis is performed on the examples of BFG beams with various boundary conditions and slenderness ratios. The obtained results are compared with the previously published results in order to show the accuracy and effectiveness of the present approach. The effects of number of elements, boundary conditions and slenderness ratios on the optimized natural frequencies of BFG beams are investigated.

Key words: bidirectional functionally graded beam, non-uniform rational b-spline, optimization, natural frequency, differential evolution.

1. Introduction

Recently, functionally graded materials (FGMs) in which the volume fractions of material constituents vary gradually along a certain direction have received great attention in many engineering fields such as aerospace, aircraft, automobile, defense industries, nuclear power plants and semiconductor technologies due to their superior mechanical and thermal properties. The main advantages of FGMs against the classical composites are that the delamination, stress concentrations and residual stresses can be avoided, and thus structural integrity can be maintained to a desirable level.

Up to the present, considerable research effort has been made for development of the free vibration analysis of beams made of FGMs. Pradhan and Chakraverty [1] performed the free vibration analysis of FG beams subjected to different sets of boundary conditions by means of the Rayleigh-Ritz method. To study the effects of shear deformation, gradient index and slenderness ratio on the natural frequencies of FG beams, the analysis was based on the classical and first-order shear deformation beam theories. They found that the natural frequency decreased if the material was towards metal or the span-to-height ratio became smaller. A finite beam element model was developed by Vo *et al.* [2] based on a quasi-3D theory to investigate the free vibration and buckling behavior of FG sandwich beams in which both shear deformation and thickness stretching effects are included. Thai and Vo [3] presented various higher-order shear deformation beam theories for bending and free vibration of FG beams considering the transverse shear strain which satisfied the stress-free boundary conditions on top and bottom surfaces. For a FG beam with a circular cross-section of an arbitrary radial gradient, Huang and Li [4] established a higher-order theory of beams including shear deformation and rotary inertia where the traction-free surface condition was identically met. Şimęk [5] employed different higher-order beam theories to compute the fundamental frequency. The classical beam theory and different higher-order shear deformation theories were used by Aydogdu and Taskin [6] for the free vibration analysis of FG beams with simply supported edges. They used the Navier type solution method to obtain natural frequencies. A Carrera Unified Formulation (CUF) was used by Mashat *et al.* [7] to perform the free vibration of FG layered beams by various theories and finite elements. The displacement components were defined by using a variety of functions such as polynomials, trigonometric, hyperbolic and exponential. Li *et al.* [8] analyzed the free vibration of axially non-homogeneous beams. The characteristic equations were derived in a closed-form for exponentially graded beams with various end conditions. They sought the minimal natural frequency for a certain gradient index, and this helps engineering to optimal design vibrating non-homogeneous beam structures. Jin and Wang [9] established successfully a novel N-node quadrature thin FG beam element based on the classical beam theory with combinations of boundary conditions to obtain the accurate natural frequency of Euler-Bernoulli FG beams. A new beam theory different from the traditional first-order shear deformation beam theory was used by Sina *et al.* [10] to analyze the free vibration of FG beams. They investigated the effects of various boundary conditions, gradient index and span-to-height ratio.

From the previously cited references, it is seen that most of previous studies are related to the free vibration analysis of FG beams whose material properties vary in only one direction. As pointed out in the study by Nemat-Alla [11], the conventional FGMs are not efficient in some engineering applications such as aerospace shuttles and craft since the temperature or stress distribution in structural elements of such advanced machines can be in two or three directions. Due to this fact, there is a need for a new type of FGMs whose material properties vary in two or three directions to obtain more effective high-temperature resistant materials. However, there have been a very little number of studies related on FG beams with two-dimensional dependent material properties so far. Lü *et al.* [12] proposed a novel elasticity solution using the state-space-based differential quadrature method for static bending and thermal deformations of bidirectional functionally graded (BFG) beams whose properties are varied exponentially. Zhao *et al.* [13] presented a symplectic elasticity solution based on the state-space formalism for static and free vibration analyses of BFG beams with elasticity modulus varying exponentially in both axial and thickness directions. The free and forced vibration of a BFG beam under a moving load has been studied by Şimşek [14] using the Ritz method for the case that the material properties of beam vary exponentially in the thickness and length directions. Şimşek [15] also investigated the buckling response of a BFG beam on the basis of the Timoshenko beam theory using the Ritz method. In order to obtain buckling load, the trial functions for axial, transverse deflections and rotation of cross-sections were expressed in polynomial forms. Wang *et al.* [16] derived the closed-form characteristic equations to study the free vibration analysis of Euler–Bernoulli BFG beams with a power law gradation of the elastic modulus, material density along the beam length and an exponential gradation along the beam thickness. It was shown that there existed an abrupt jump for the natural frequencies of BFG beams depending on the gradient parameter. Hao and Wei [17] proposed a new method to directly form an exact dynamic stiffness matrix by using state space differential equations. The natural frequency of a BFG beam was computed by combining the Wittrick–Williams algorithm with a non-iterative algorithm.

It is noted that the performance of a FG component is not only a function of the material properties, but is directly related to the ability of the designer to utilize the materials in the most optimal fashion. Until now, a few research efforts have been directed toward the design of FG beams for optimal natural frequencies. Goupee and Vel [18] presented a new methodology for the simulation and optimization of the two-dimensional steady-state free and forced vibration of BFG beams based on the element-free Galerkin method. Qian and Ching [19] and Qian and Batra [20] have sought to maximize the frequencies of a cantilever FG beam. Roque and Martins [21] used the differential evolution (DE) optimization to find the volume fraction that maximized the first natural frequency of a FG beam. A formulation using three parameters was employed to describe the volume fraction. Roque *et al.* [22] also used the DE algorithm to design the simply supported and cantilever FG nano beams in order to obtain the lowest free vibration frequency based on a modified couple stress theory. Recently, Tsiatas and Charalampakis [23] have proposed a method to optimize the natural frequencies of axially functionally graded beams and arches by tailoring appropriately their material distribution. The DE algorithm was employed for optimizing the natural frequencies.

The isogeometric analysis (IGA) which is used in this study has been proposed by Hughes *et al.* [24] to bridge the gap between computer aided design (CAD) and finite element analysis (FEA). The main idea of IGA is to adopt the CAD basis functions (e.g., NURBS) to be the shape functions in FEA to construct the approximation of the field variables and to describe the geometry of engineering components used for analysis. A distinct advantage over FEM is that the mesh refinement is not only simply accomplished by the automatic communication with the CAD geometry tools, but leaves the geometry intact. Another intriguing trait of these functions is that they are typically smooth beyond the classical C^0-continuity of the standard FEM. Comprehensive knowledge of IGA could be found in the text book of Cottrell *et al.* [25]. The IGA-based approaches have been used to solve many problems in a wide range of research areas including beams [26–30], plates [31–33] and shells [34–37]. However, to the authors' knowledge, there are no reported experiments on the optimization of natural frequency for FG beams by using IGA in the literature.

The objective of this paper is to present the NURBS-based IGA in order to find the optimum volume fractions that maximize the natural frequencies of W/Cu BFG beams. The IGA is utilized for the numerical simulation of the free vibration of BFG beams. To construct the geometry of a beam as well as approximate solutions, one-dimensional NURBS basis functions are employed, whereas two-dimensional basis functions are represented for the gradation of material properties. The differential evolution (DE) algorithm is used to optimize the volume fraction distributions that maximize each of the first three natural frequencies of BFG beams. Numerical examples are presented for the free vibration and optimization analysis of BFG beams. The obtained results are compared with the previously published results in order to show the accuracy and effectiveness of the present approach. In particular, the effects of number of elements, boundary conditions and slenderness ratios on the optimized natural frequencies of BFG beams are studied.

The paper is organized as follows: next section describes a FG material featuring. In Section 3, the theory and formulation of BFG beam are presented. A brief review on the NURBS-based IGA is given in Section 4. Section 5 provides the principle of optimization algorithm. The numerical results and discussions are presented in Section 6. Finally, the article is closed with some concluding remarks.

2. Bidirectional functionally graded material

The BFG beams with length L, width b and thickness h are considered as shown in Fig. 1. The BFG beams are made of a continuous gradation of at least two distinct material phases whose properties are assumed to be changed smoothly along the longitudinal and thickness directions, respectively.

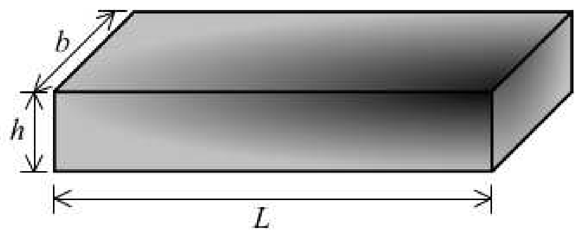

Fig. 1. Schematic view of BFG beam.

To optimize the material composition, in this study, the Mori–Tanaka method [38] is used for estimating the effective properties of two-phase FGMs. This method assumes that the matrix phase is reinforced with spherical inclusions and accounts for the interplay of the elastic fields between neighboring particles. According to the Mori–Tanaka homogenization method, the effective bulk modulus K and shear modulus G of the BFG beam are evaluated as [38, 39]:

$$\frac{K-K_m}{K_c-K_m}=\frac{V_c}{1+(1-V_c)\frac{3(K_c-K_m)}{3K_m+4G_m}}, \tag{2.1a}$$

$$\frac{G-G_m}{G_c-G_m}=\frac{V_c}{1+(1-V_c)\frac{(G_c-G_m)}{G_m+f_1}}, \tag{2.1b}$$

where

$$f_1=\frac{G_m(9K_m+8G_m)}{6(K_m+2G_m)}. \tag{2.2}$$

In which V_c is the volume fraction of the ceramic phase. The subscripts c and m refer to the ceramic and metal phases, respectively. The volume fractions of the ceramic and metal phases are related by $V_c+V_m=1$. The effective Young's modulus E and Poisson's ratio ν can be expressed as

$$E(x,z)=\frac{9KG}{3K+G}, \tag{2.3a}$$

$$\nu(x,z)=\frac{3K-2G}{2(3K+G)}. \tag{2.3b}$$

The effective mass density ρ is given by the rule of mixture as

$$\rho(x,z) = \rho_c V_c + \rho_m V_m. \tag{2.4}$$

It is noted that the effective material properties such as K, G, E, ν and ρ vary in both axial and thickness directions.

3. Theory and formulation

In the Timoshenko beam theory, the plane cross-section remains plane but not necessarily normal to the neutral axis after deformation. Therefore, the effect of shear deformation can be taken into account in the analysis. The displacement field can be expressed as

$$u_x(x,z,t) = u(x,t) + z\varphi(x,t), \tag{3.1a}$$

$$u_z(x,z,t) = w(x,t), \tag{3.1b}$$

where u and w denote the axial and transverse displacements, respectively, of any point on the neutral axis; φ is the rotation of the cross-section. With the geometrical and physical linearity assumptions, the strains and stresses of BFG beam take the following form:

$$\varepsilon_{xx} = \frac{\partial u(x,t)}{\partial x} + z\frac{\partial \varphi(x,t)}{dx}, \tag{3.2a}$$

$$\gamma_{xz} = \frac{\partial w(x,t)}{\partial x} + \varphi(x,t), \tag{3.2b}$$

$$\sigma_{xx} = E(x,z)\,\varepsilon_{xx}, \tag{3.2c}$$

$$\sigma_{xz} = k_s G(x,z)\gamma_{xz}, \tag{3.2d}$$

where ε_{xx} and γ_{xz} are the longitudinal strain and the transverse shear strain, respectively; σ_{xx} and σ_{xz} are the axial normal stress and the shear stress, respectively; k_s is the shear correction factor. The internal strain energy of a beam at any instant in terms of stresses and strains can be expressed by

$$U_i = \frac{1}{2}\int_V (\sigma_{xx}\varepsilon_{xx} + \sigma_{xz}\gamma_{xz})\,dV, \tag{3.3}$$

where V is the volume of beam. Substituting Eq. (3.2) into Eq. (3.3) yields

$$U_i = \frac{1}{2}\int_{-L/2}^{L/2} \left[A_{xx}\left(\frac{\partial u}{\partial x}\right)^2 + 2B_{xx}\frac{\partial u}{\partial x}\frac{\partial \varphi}{\partial x} + k_s A_{xz}\left(\frac{\partial w}{\partial x} + \varphi\right)^2 + D_{xx}\left(\frac{\partial \varphi}{\partial x}\right)^2\right] dx, \tag{3.4}$$

where

$$(A_{xx}, B_{xx}, D_{xx}) = \int\limits_{-h/2}^{h/2} E(x,z)(1,z,z^2)b\,dz, \tag{3.4a}$$

$$A_{xz} = \int\limits_{-h/2}^{h/2} G(x,z)\,bdz. \tag{3.4b}$$

With a similar procedure, the kinetic energy of the BFG beam can be obtained as

$$K_e = \frac{1}{2}\int\limits_{-L/2}^{L/2}\left[I_a\left(\frac{\partial u}{\partial t}\right)^2 + I_a\left(\frac{\partial w}{\partial t}\right)^2 + 2I_b\frac{\partial u}{\partial t}\frac{\partial \varphi}{\partial t} + I_d\left(\frac{\partial \varphi}{\partial t}\right)^2\right]dx, \tag{3.5}$$

where t is the time and the internal coefficient appearing in Eq. (3.5) is given as

$$(I_a, I_b, I_d) = \int\limits_{-h/2}^{h/2} \rho(x,z)(1,z,z^2)b\,dz. \tag{3.6}$$

To derive the equations of motion, the Hamilton's principle is adopted herein as

$$\int\limits_{t_1}^{t_2} (\delta U_i - \delta K_e)\,dt = 0, \tag{3.7}$$

where the variational forms of strain energy U_i and kinetic energy K_e can be expressed as follows:

$$\delta U_i = \int\limits_{-L/2}^{L/2}\left[\delta\frac{\partial u}{\partial x}\left(A_{xx}\frac{\partial u}{\partial x} + B_{xx}\frac{\partial \varphi}{\partial x}\right) + \delta\frac{\partial \varphi}{\partial x}\left(B_{xx}\frac{\partial u}{\partial x} + D_{xx}\frac{\partial \varphi}{\partial x}\right)\right.$$
$$\left. + k_s A_{xz}\left(\delta\frac{\partial w}{\partial x} + \delta\varphi\right)\left(\frac{\partial w}{\partial x} + \varphi\right)\right]dx, \tag{3.8a}$$

$$\delta K_e = \int\limits_{-L/2}^{L/2}\left[\delta\frac{\partial u}{\partial t}\left(I_a\frac{\partial u}{\partial t} + I_b\frac{\partial \varphi}{\partial t}\right) + \delta\frac{\partial w}{\partial t}I_a\frac{\partial w}{\partial t}\right.$$
$$\left. + \delta\frac{\partial \varphi}{\partial t}\left(I_b\frac{\partial u}{\partial t} + I_d\frac{\partial \varphi}{\partial t}\right)\right]dx. \tag{3.8b}$$

Then the following governing equations are achieved by taking the variation of displacement components and integrating by parts as

$$A_{xx}\frac{\partial^2 u}{\partial x^2}+B_{xx}\frac{\partial^2 \varphi}{\partial x^2}-I_a\frac{\partial^2 u}{\partial t^2}-I_a\frac{\partial^2 \varphi}{\partial t^2}=0, \tag{3.9a}$$

$$k_s A_{xx}\left(\frac{\partial^2 w}{\partial x^2}+\frac{\partial \varphi}{\partial x}\right)-I_a\frac{\partial^2 w}{\partial t^2}=0, \tag{3.9b}$$

$$B_{xx}\frac{\partial^2 u}{\partial x^2}+D_{xx}\frac{\partial^2 \varphi}{\partial x^2}-k_s A_{xx}\left(\frac{\partial w}{\partial x}+\varphi\right)-I_b\frac{\partial^2 u}{\partial t^2}-I_d\frac{\partial^2 \varphi}{\partial t^2}=0. \tag{3.9c}$$

4. NURBS-based isogeometric analysis

In this study, one-dimensional (1D) NURBS basis functions are used to construct exactly the geometry as well as approximate solution, while a material property variation is described by the 2D NURBS surface. An overview of the NURBS basis function construction is briefly discussed as a prelude to the description of the solution field approximation for the NURBS-based isogeometric analysis. For more detail, one can refer to the book of Cottrell *et al.* [25].

4.1. NURBS basis functions

The primary component of the NURBS basis function is a knot vector $\Xi = \{\xi_1, \xi_2, \ldots, \xi_{n+p+1}\}$ which is a set of non-decreasing sequence of parameter values of ξ_i, $i = 1, 2, \ldots, n+p+1$, where $\xi_i \in \mathbb{R}$ is called ith knot in the parameter space, n is the number of basis functions and p is the order of B-Spline. The first and last knots are repeated $p+1$ times in the so-called open knot vector. Basis functions by the open knot vector are interpolatory at the beginning and end of the parametric space interval. This distinguishes the knots from the nodes in the finite element analysis as all the nodes are interpolatory. Based on an uniform open knot vector Ξ, B-Spline basis functions are constructed recursively using the Cox-DeBoor algorithm as follows ($p = 0$):

$$N_{i,0}(\xi)=\begin{cases}1 & if\ \xi_i \le \xi \le \xi_{i+1},\\ 0 & \text{otherwise.}\end{cases} \tag{4.1}$$

And basis functions for orders $p = 1, 2, \ldots,$ are defined as

$$N_{i,p}(\xi)=\frac{\xi-\xi_i}{\xi_{i+p}-\xi_i}N_{i,p-1}(\xi)+\frac{\xi_{i+p+1}-\xi}{\xi_{i+p+1}-\xi_{i+1}}N_{i+1,p-1}(\xi). \tag{4.2}$$

An important property of B-Spline basis functions is that they constitute a partition of a unit, $\sum_{i=1}^{n} N_{i,p}(\xi) = 1, \forall\xi$, that makes the B-Spline basis possible to become the basis for the approximate displacement field.

The one-dimensional (1D) rational basis function $R_i^p(\xi)$ and NURBS curve $C(\xi)$ are defined by a weighted average of the B-Spline basis functions as follows:

$$R_i^p(\xi) = \frac{N_{i,p}(\xi)w_i}{\sum_{j=1}^{n} N_{j,p}(\xi)w_i}, \tag{4.3}$$

$$C(\xi) = \sum_{i=1}^{n} R_i^p(\xi)B_i, \tag{4.4}$$

where w_i, $i = 1, 2, \ldots, n$ are the ith weight, $0 < w_i \le 1$; $B_i \in \mathbb{R}$, $i = 1, 2, \ldots, n$ are the control points in the ξ direction.

Similarly, the two-dimensional (2D) NURBS basis functions can be constructed by taking the tensor product of two 1D B-Spline basis functions as

$$R_{i,j}^{p,q}(\xi,\eta) = \frac{N_{i,p}(\xi)M_{j,q}(\eta)w_{i,j}}{\sum_{i=1}^{n}\sum_{j=1}^{m} N_{i,p}(\xi)M_{j,p}(\eta)w_{i,j}}, \tag{4.5}$$

where $R_{i,j}^{p,q}(\xi,\eta)$ represents the bivariate NURBS basis functions; $N_{i,p}(\xi)$ and $M_{j,q}(\eta)$ stand for the B-Spline basis functions of order p in the ξ direction and order q in the η direction, respectively; $w_{i,j}$ denotes the 2D weight and m is the number of control points in η direction.

By using the NURBS basis functions, a NURBS surface of order p in the ξ direction and order q in the η direction can be expressed as

$$S(\xi,\eta) = \sum_{i=1}^{n}\sum_{j=1}^{m} R_{i,j}^{p,q}(\xi,\eta)B_{i,j}, \tag{4.6}$$

where $B_{i,j}$ is the control mesh of $n \times m$ control points in two directions.

The first derivative of $R_{i,j}^{p,q}(\xi,\eta)$ with respect to each parametric variable, e.g., ξ, is derived by applying the quotient rule to Eq. (4.5) as

$$\frac{\partial R_{i,j}^{p,q}(\xi,\eta)}{\partial \xi} = \frac{\frac{\partial N_{i,j}(\xi)}{\partial \xi} M_{j,q}(\eta)w_{i,j}W(\xi,\eta) - \frac{\partial W(\xi,\eta)}{\partial \xi} N_{i,p}(\xi)M_{j,q}(\eta)w_{i,j}}{[W(\xi,\eta)]^2}, \tag{4.7}$$

where

$$W(\xi,\eta) = \sum_{i=1}^{n}\sum_{j=1}^{m} N_{i,p}(\xi)M_{j,q}(\eta)w_{i,j}, \tag{4.8}$$

$$\frac{\partial W(\xi,\eta)}{\partial \xi} = \sum_{i=1}^{n}\sum_{j=1}^{m} \frac{\partial N_{i,p}(\xi)}{\partial \xi} M_{j,q}(\eta)w_{i,j}. \tag{4.9}$$

4.2. NURBS-based BFGM modelling

As stated previously, the material property variations of BFG beam are described by 2D NURBS basis functions in Eq. (4.5) as follows:

$$\Re(\xi,\eta)=\sum_{i=1}^{n}\sum_{j=1}^{m}R_{i,j}^{p,q}(\xi,\eta)\Re_{i,j}, \tag{4.10}$$

where $\Re_{i,j}$ are the values of material properties at corresponding control points as shown in Fig. 2. In the isogeometric concept, the net of control points for interpolation of material properties throughout the domain of BFG beam is intended to use separately with geometry and analysis. The control mesh based on 4×4 2D NURBS elements which are employed to describe material properties is shown in Fig. 2 with the knot vectors $\Xi=\{0,0,0,1/2,1,1,1\}$ and $\Psi=\{0,0,0,1/3,2/3,1,1,1\}$ with orders $p=2$ and $q=2$, respectively.

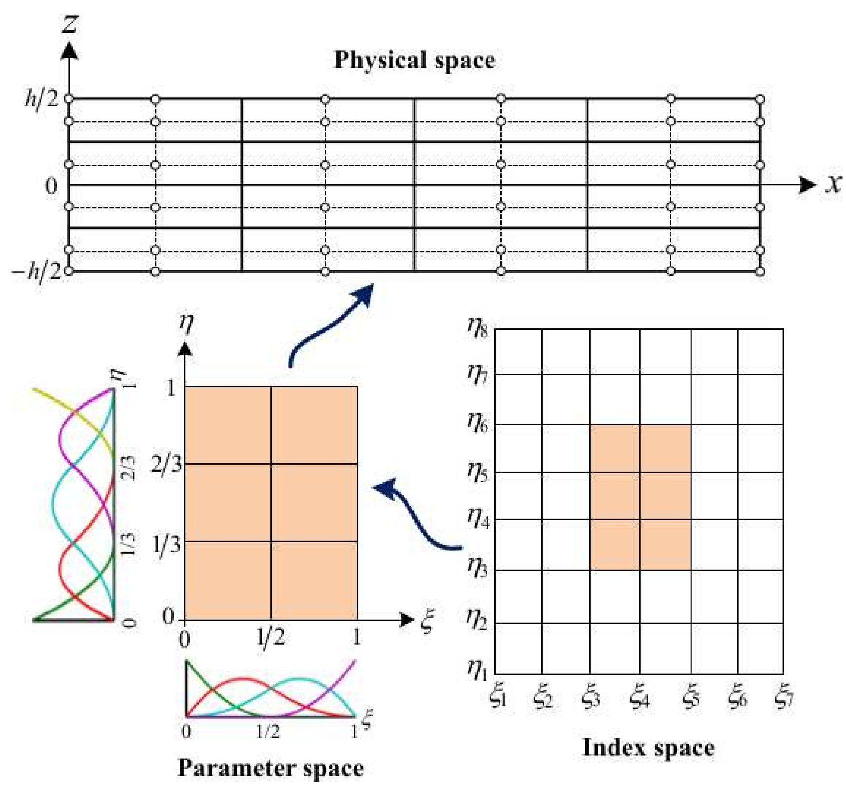

Fig. 2. Schematic illustration of NURBS-based isogeometric BFG beam (4×4 NURBS elements, $p=2$, $q=2$).

4.3. Isogeometric finite element discretization

The parametric domain in the isogeometric analysis is similar to the isoparametric space in the classical finite element method. Thus, the generalized displacement measures are approximated by the NURBS basis functions defined above as follows:

$$u(\xi) = \sum_{i=1}^{n} R_i^p(\xi) u_0, \tag{4.11a}$$

$$w(\xi) = \sum_{i=1}^{n} R_i^p(\xi) w_0, \tag{4.11b}$$

$$\varphi(\xi) = \sum_{i=1}^{n} R_i^p(\xi)\, \varphi_0. \tag{4.11c}$$

By substituting Eq. (4.13) into Eq. (3.7), the isogeometric finite element model of a typical element can be expressed as

$$\mathbf{M}\ddot{\mathbf{u}} + \mathbf{K}\mathbf{u} = 0, \tag{4.11}$$

where $\mathbf{K}$ and $\mathbf{M}$ are the stiffness and mass matrices, respectively; $\mathbf{u}$ is the vector of the degrees of freedom associated to the displacement field. The explicit forms of stiffness and mass matrices are given by

$$\mathbf{K} = \begin{bmatrix} \mathbf{K}^{11} & \mathbf{K}^{12} & \mathbf{K}^{13} \\ \mathbf{K}^{21} & \mathbf{K}^{22} & \mathbf{K}^{23} \\ \mathbf{K}^{31} & \mathbf{K}^{32} & \mathbf{K}^{33} \end{bmatrix}, \tag{4.12}$$

where

$$\begin{aligned}
K_{ij}^{11} &= \int_{L_e}^{L_{e+1}} A_{xx} R_i' R_j' dx, \qquad K_{ij}^{12} = K_{ji}^{21} = 0, \\
K_{ij}^{13} &= K_{ji}^{31} = \int_{L_e}^{L_{e+1}} B_{xx} R_i' R_j' dx, \\
K_{ij}^{22} &= \int_{L_e}^{L_{e+1}} A_{xz} R_i' R_j' dx, \qquad K_{ij}^{23} = K_{ji}^{32} = 0, \\
K_{ij}^{33} &= \int_{L_e}^{L_{e+1}} (A_{xz} R_i R_j + D_{xx} R_i' R_j')\, dx,
\end{aligned} \tag{4.13}$$

and

$$\mathbf{M} = \begin{bmatrix} \mathbf{M}^{11} & \mathbf{M}^{12} & \mathbf{M}^{13} \\ \mathbf{M}^{21} & \mathbf{M}^{22} & \mathbf{M}^{23} \\ \mathbf{M}^{31} & \mathbf{M}^{32} & \mathbf{M}^{33} \end{bmatrix}. \tag{4.14}$$

where

$$\begin{aligned} M_{ij}^{11} &= M_{ij}^{22} = \int\limits_{L_e}^{L_{e+1}} I_a R_i R_j dx, \quad M_{ij}^{12} = M_{ji}^{21} = 0, \\ M_{ij}^{13} &= M_{ji}^{31} = \int\limits_{L_e}^{L_{e+1}} I_b R_i R_j dx, \\ M_{ij}^{23} &= M_{ji}^{32} = 0, \quad M_{ij}^{33} = \int\limits_{L_e}^{L_{e+1}} I_d R_i R_j dx, \end{aligned} \tag{4.15}$$

where the prime represented differentiation with respect to x. After substituting the characteristic of the time function $\ddot{\mathbf{u}} = -\omega^2 \mathbf{u}$, the following algebraic equation is obtained:

$$(\mathbf{K} - \omega^2 \mathbf{M})\, \mathbf{u} = 0, \tag{4.16}$$

where ω is the natural frequency. The natural frequencies are obtained using the standard generalized eigenvalue algorithm. The assembly of two matrices follows the standard procedure of FEM.

5. Differential evolution algorithm

The differential evolution (DE) is a unique evolutionary algorithm designed to deal with continuous optimization problems. Similar to GA, the DE is a population-based algorithm that is stochastic in nature to find global solution in feasible individual space. The main procedure of DE includes four phases such as initiation, mutation, crossover and selection.

5.1. Initialization

In the DE algorithm, each individual in the population is the d-dimensional vector that represents a candidate solution to the problem and is randomly created in the search domain as

$$x_{ij} = x_j^L + r \times (x_j^U - x_j^L), \qquad i = 1, 2, \ldots, NP; \quad j = 1, 2, \ldots, d, \tag{5.1}$$

where x_{ij} is the jth component of individual $\mathbf{x}_i$; x_j^U and x_j^L are the upper and lower bounds of x_j, respectively; r is a uniformly distributed random number in the interval $[0, 1]$; NP is the size of population and d is the number of design variables.

5.2. Mutation

In the mutation phase, the basic idea of DE is presented as follows: taking the difference vector between two individuals and adding a scaled version of the difference vector to the third individual to create a new candidate solution [40]. The process is described as follows:

$$\mathbf{v}_i = \mathbf{x}_{r1} + F \times (\mathbf{x}_{r2} - \mathbf{x}_{r3}), \tag{5.2}$$

where $\mathbf{v}_i$ is a mutation vector and known as a new candidate solution; $\mathbf{x}_{r1}$, $\mathbf{x}_{r2}$ and $\mathbf{x}_{r3}$ are candidate solutions; r_1, r_2 and r_3 are randomly selected from $(1, 2, \ldots, NP)$ to satisfy the following constraints as $r_1 \neq r_2 \neq r_3 \neq i$; the scaling factor F can be chosen in the range $F \in [0, 2]$.

5.3. Crossover

Next, the trial vector $\mathbf{u}_i$ is defined by combining the mutant vector $\mathbf{v}_i$ with a DE individual $\mathbf{x}_i$, given as

$$u_{ij} = \begin{cases} v_{ij} & \text{if } r_{cj} < C_r, \\ x_{ij} & \text{otherwise}, \end{cases} \tag{5.3}$$

in which r_{cj} is a random number taken from the uniform distribution $[0, 1]$; C_r is a constant crossover rate chosen in the range $[0, 1]$, which controls how likely it is that each component of $\mathbf{u}_i$ comes from the mutant vector $\mathbf{v}_i$ and is defined by a user.

5.4. Selection

Finally, the $\mathbf{u}_i$ and $\mathbf{x}_i$ vectors are compared so that the most fit vector in each pair is kept for the next generation and the least fit is discarded. This step is a greedy selection criterion, which for a minimization problem is expressed as

$$\mathbf{x}_i^{\text{new}} = \begin{cases} \mathbf{u}_i & \text{if} f(\mathbf{u}_i) \leq f(\mathbf{x}_i), \\ \mathbf{x}_i & \text{otherwise}, \end{cases} \tag{5.4}$$

where $f(\mathbf{u}_i)$ and $f(\mathbf{x}_i)$ are the objective function values.

5.5. Optimization problem

In an optimization formulation, the optimized material distribution of a two-phase FGM is equivalent to the determination of the volume fraction distribution $V(x,z)$ of one of its constituents. The volume fraction at an arbitrary point in the domain is obtained by interpolation of the volume fraction values defined at the control points. The range-restricted interpolation ensures that the volume fractions lie in the range of zero to one at all points within the domain, i.e., $0 \leq V(x,z) \leq 1$. A constrained optimization problem is written in the following form [18]:

$$\begin{aligned} &\text{Find} && V^{(i,j)}, \quad i=1,2,\ldots,n,\; j=1,2,\ldots, \\ &\text{Minimize} && f(V^{(i,j)}), \\ &\text{Subjected to} && 0 \leq V^{(i,j)} \leq 1, \end{aligned} \tag{5.5}$$

where $f(V^{(i,j)})$ is the objective function. In the above problem, there are $n \times m$ optimization variables.

6. Numerical results and discussions

In this section, in order to verify the accuracy of present study, the NURBS-based isogeomeric optimization analysis of BFG beams is performed. The numerical results obtained are compared with the reference solutions. The effects of number of elements, boundary conditions and slenderness ratio on the optimized natural frequencies of BFG beams are investigated.

6.1. Verification

In the first part of this section, the NURBS-based isogeometric analysis code is validated by comparing the numerical results with the available solutions for FG and BFG beams. First, two types of FG beams are considered. One for that the material properties of the beam varing continuously in an axial direction and the other is devoted to material properties which are changed continuously in the thickness direction. In case of variation through the axial direction, the left side is pure alumina (Al_2O_3) and the right side is pure iron (Fe). The material properties vary according to a power law as $\Re(x) = (\Re_l - \Re_r)(1 - x/L)^{k1} + \Re_r$. In case of variation through thickness, the top surface of a beam is pure alumina, whereas the bottom surface of a beam is pure iron with $\Re(z) = (\Re_t - \Re_b)(1/2 + z/h)^{k3} + \Re_b$. The geometry and material properties are presented in Alshorbagy *et al.* [41]. The NURBS basis functions used are $p = 3$ and $q = 3$ in ξ and η directions, respectively, the number of control points is 121 (11×11) and the number of elements is 64 ($e_x = 8$, $e_z = 8$).

For the simply supported (SS) FG beam with $L/h = 20$, the first two dimensionless frequencies are depicted in Figs. 3 and 4 with respect to k_1 and k_3, respectively, for different material distribution. The ratio of mass densities of

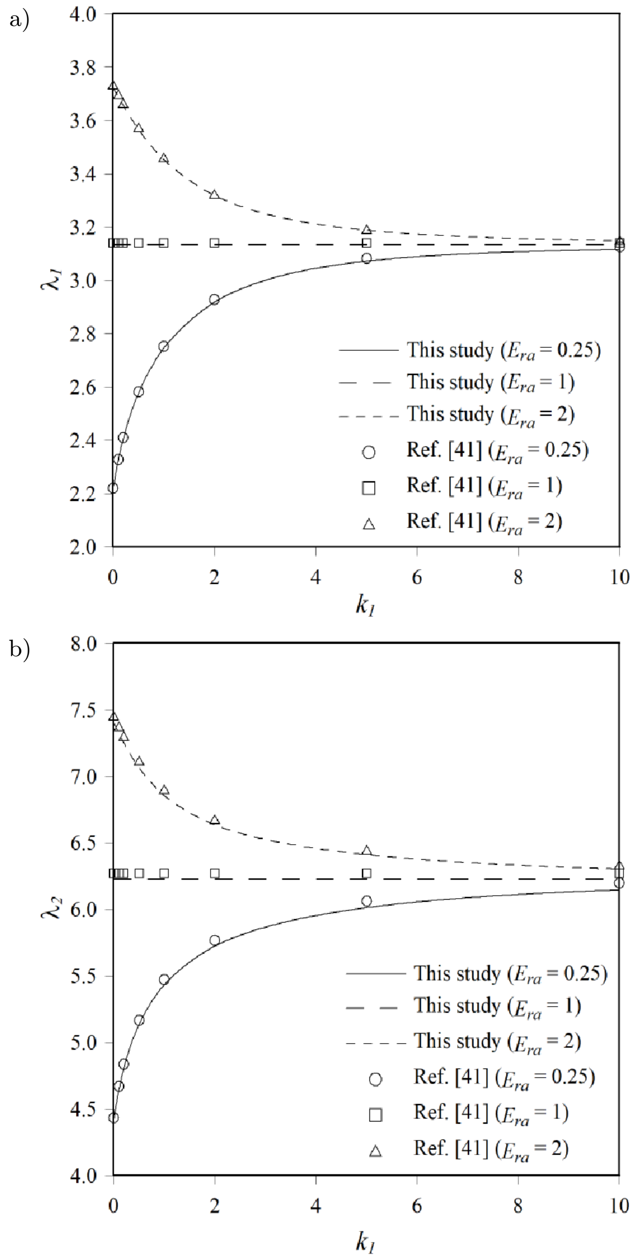

Fig. 3. The first two dimensionless frequencies of SS FG beam with respect to k_1 for differential material distribution; a) mode 1, b) mode 2.

alumina to iron is $\rho_{ra} = \rho_l/\rho_r = \rho_t/\rho_b = 1$ and the ratios of Young's moduli of alumina to iron are $E_{ra} = E_l/E_r = E_t/E_b = 0.25$, 1 and 2. For convenience,

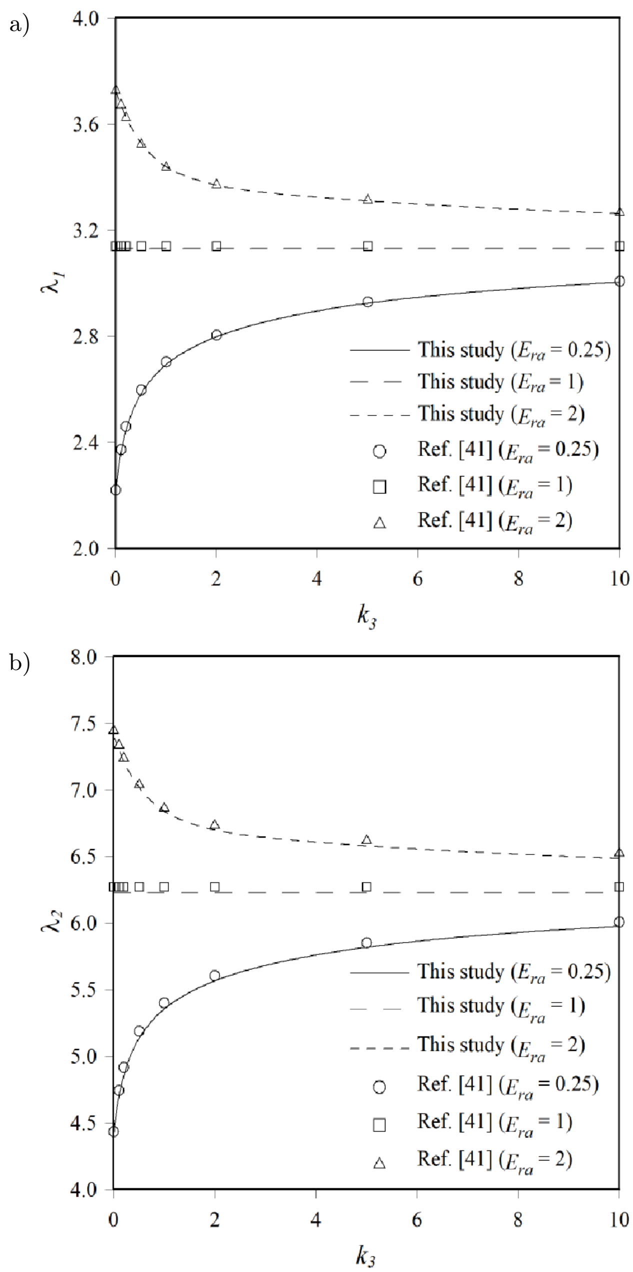

Fig. 4. The first two dimensionless frequencies of SS FG beam with respect to k_3 for differential material distribution; a) mode 1, b) mode 2.

the following dimensionless frequency is used: $\lambda_i^2 = \omega_i L^2 \sqrt{\rho_l A/(E_l I)}$. It can be observed from Figs. 3 and 4 that the results from this study agree well with those from ALSHORBAGY *et al.* [41] using the finite element method based on the Euler-Bernoulli beam theory for both power exponents. It is seen that the natural frequencies increase with an increase in power exponent when $E_{ra} < 1$, and decrease with an increase in power exponent when $E_{ra} > 1$ for both cases. The remarkable difference between the natural frequencies due to k_1 and k_3 is not found. Figure 5 shows the convergence rate of the normalized frequencies with various orders of NURBS basis functions in ξ direction ($q = 2$). It can be realized from Fig. 5 that by using the h-refinement, the accuracy of the present isogeometric analysis solution increases as the number of elements is increased from 4 to 64. The more efficient technique, the k-refinement creating higher order, higher continuity of NURBS basis functions gives a faster convergence speed. With the aid of k-refinement, the normalized frequency converges with 4 quartic or quintic elements, and 8 cubic elements.

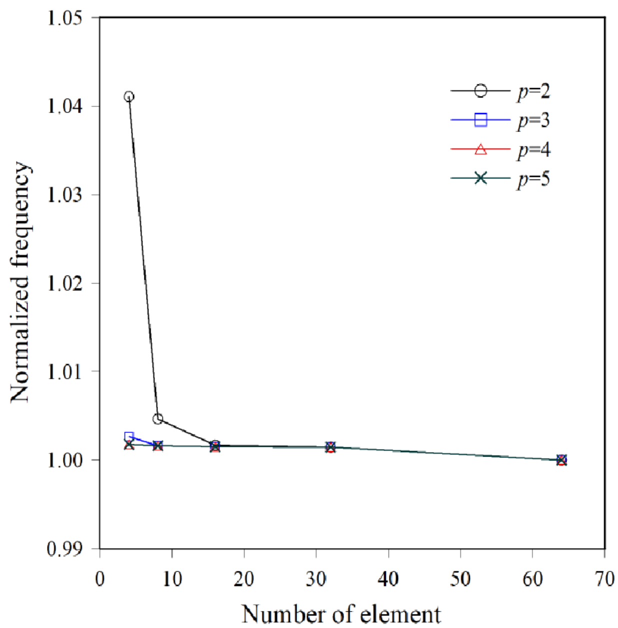

FIG. 5. Convergence of the first normalized frequencies of SS FG beam for various values of p ($q = 2$).

Next, the natural frequencies of BGF beams with various boundary conditions are evaluated. The material characteristics vary exponentially in both directions as $\Re(x, z) = \Re_{lb} e^{k1x/L+k3(0.5+z/h)}$, where $\Re_{lb}$ is the reference material value at the point (0, 0), and the material and geometrical properties are as follows: $E_{lb} = 210$ GPa, $v_{lb} = 0.3$, $\rho_{lb} = 7.850$ kg/m^3, $b = 0.5$ m, $h = 1$ m and

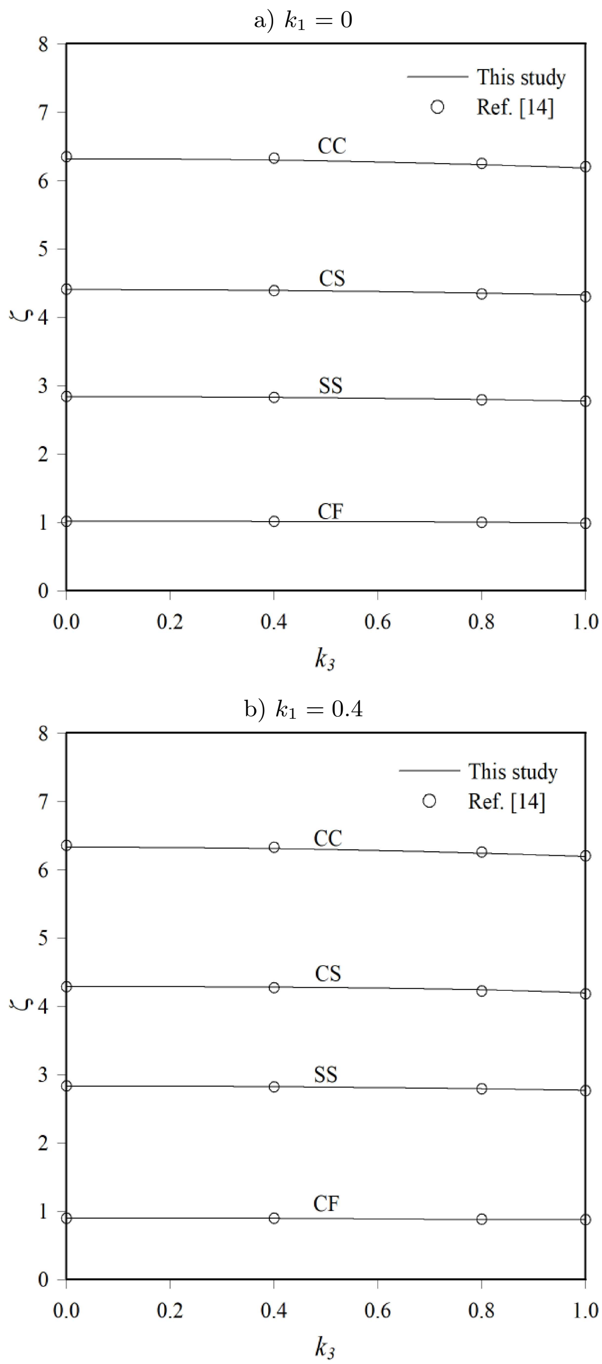

FIG. 6. The first two dimensionless frequencies of SS FG beam with respect to k_3 for differential material distribution.

c) $k_1 = 0.8$

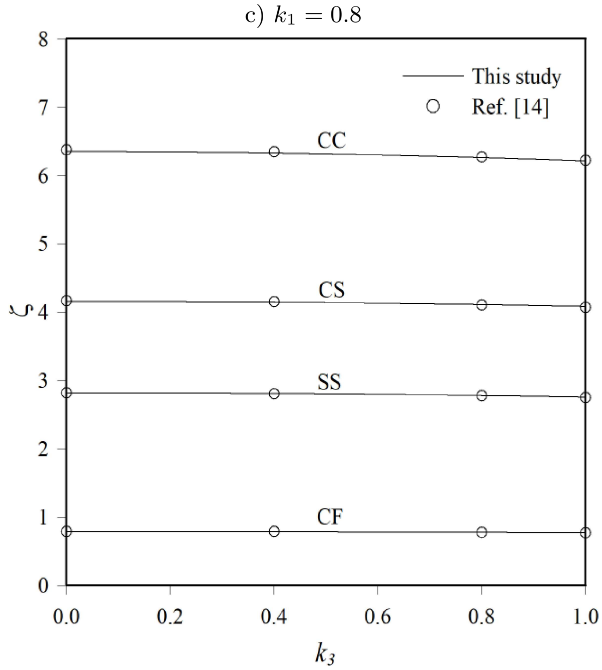

d) $k_1 = 1$

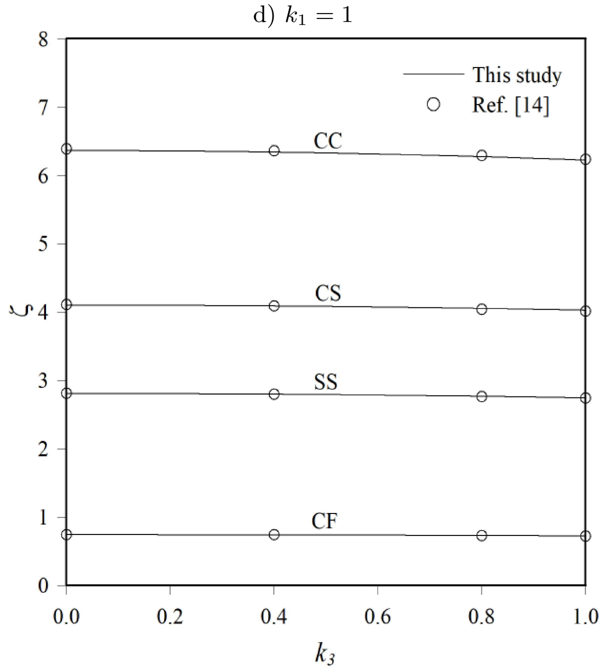

Fig. 6. [cont.] The first two dimensionless frequencies of SS FG beam with respect to k_3 for differential material distribution.

$L = 20$ m. In the analysis, CF, SS, CS and CC boundary conditions are considered, where C, F and S denote clamped, free and simple edges, respectively. The order of basis function, the numbers of control points and elements are the same as in the previous example. In Fig. 6, the first dimensionless frequencies of BGF beams with CF, SS, CS and CC end conditions are plotted and compared with those from Şimşek [14] for various values of gradient indexes. The considered dimensionless frequency is defined by $\zeta = (\omega L^2/h)\sqrt{\rho_{lb}/E_{lb}}$. It can be found from Fig. 6 that the present results are in great agreement with those from Şimşek [14] for all gradient indexes considered. It is seen that fundamental frequency values slightly decrease as the gradient indexes increase for all boundary conditions. This is due to the fact that the effect of mass density on frequency is a bit dominant than the effect of Young's modulus.

6.2. Optimization of BFG beams

In this example, the optimization of volume fraction distributions for BFG beams is considered to maximize each of the first three natural frequencies. The geometries of a beam are $h = 0.05$ m and $L = 0.2$ m and the BFG beams are composed of tungsten (W) and copper (Cu) with properties as: Tungsten (W): $E_W = 400$ GPa, $v_W = 0.28$, $\rho_W = 19{,}300$ kg/m^3; Copper (Cu): $E_{cu} = 110$ GPa, $v_{cu} = 0.34$, $\rho_{cu} = 8{,}960$ kg/m^3. To estimate the effective material properties throughout the domain, the Mori–Tanaka scheme with copper as the matrix phase is used. It is noted that the tungsten has higher stiffness and density than copper. The addition of tungsten to a copper can either increase or decrease its natural frequencies depending on where it is added. Thus, in order to obtain desired dynamic responses for a W/Cu beam, the tungsten distribution can be optimized [18]. The searching process of the present DE algorithm is stopped when the absolute value of deviation between the objective function value of the best individual and the mean objective function value of the whole population is less than or equal to tolerance 1×10^{-5}. In addition, the population size NP, the mutation scaling factor F and the crossover factor C_r for real decision parameters are set to be 20, 0.85 and 0.85, respectively.

Table 1. The first three optimized frequencies (Hz) of CF BFG beam for different number of elements ($p = 3$, $q = 2$).

Mode	This study			Goupee and Ve [18]
	$e_x = 4$	$e_x = 8$	$e_x = 16$	
1	1050.5	1158.8	1179.3	1174.3
2	4689.0	4874.9	5032.9	4819.0
3	6054.0	6578.8	6649.7	6681.9

The first three optimized frequencies obtained from this study are presented in Table 1 for CF W/Cu beam with different number of elements in x direction. In this study, the enough elements, i.e., $e_z = 16$, along z direction are used since the numerical integration is carried out with respect to the control points in η direction to construct the stiffness and mass matrices. In addition, the NURBS basis functions considered are $p = 3$ and $q = 2$ in ξ and η directions, respectively. For comparison, the solutions from Goupee and Vel [18]

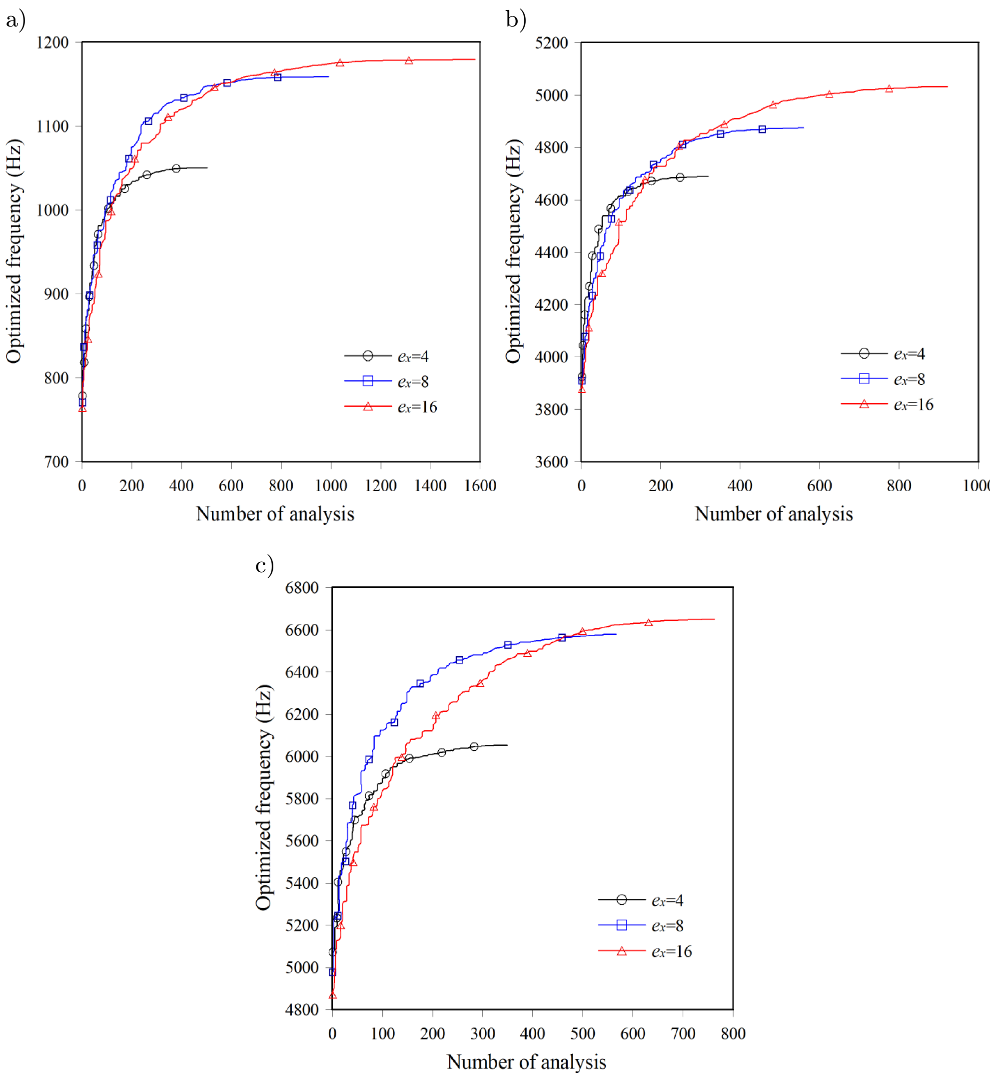

Fig. 7. Convergence of the first three optimized frequencies of CF BFG beam for various values of e_x.

based on the two-dimensional element-free Galerkin method using a total of 30 design variables and the genetic algorithm are presented. It can be observed from Table 1 that the present results using 16 elements in x direction are in good agreement with solutions from [18]. The convergence rates of the first three optimized frequencies are depicted in Fig. 7 for various numbers of elements in x direction. It is observed that in all the cases, the faster convergence exhibits as the number of element increases. It can also be found from Table 1 that the fundamental vibration mode of the optimized W/Cu beam is flexural mode and corresponding frequency is $\omega_1 = 1179.3$ Hz, compared to 674.0 Hz for a monolithic Cu beam and 877.1 Hz for a monolithic W beam, which is 75.0% larger than a monolithic copper beam and 34.5% larger than a monolithic tungsten beam. Figure 8a shows the tungsten volume fraction distribution of the optimized W/Cu beam that results in the largest fundamental frequency ω_1. It can be observed from Fig. 8a that the tungsten distribution is symmetric

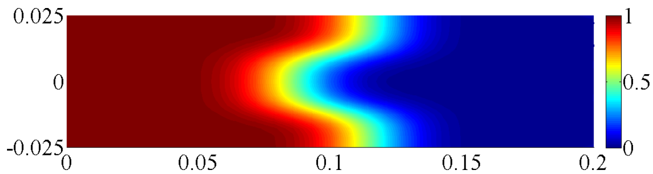

a) Mode 1 of CF beam

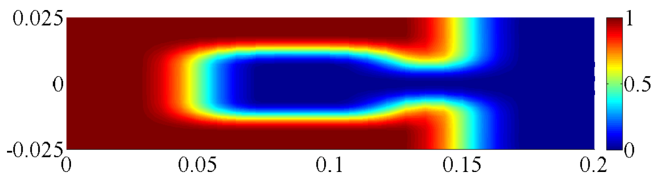

b) Mode 2 of CF beam

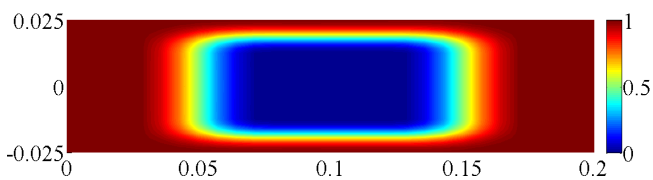

c) Mode 1 of CC beam

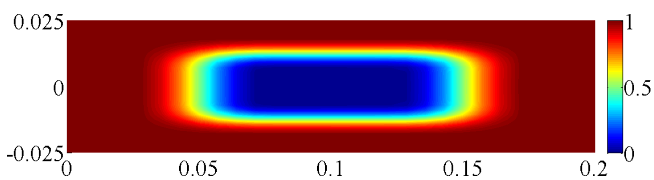

d) Mode 2 of CC beam

Fig. 8. Optimized tungsten volume fraction distributions of CF and CC BFG beams.

about the middle axis and the optimized W/Cu beam consists of the stiffer tungsten near the root and the more compliant copper at the tip. The material composition smoothly transitions from tungsten and copper with a narrow region. The optimized tungsten volume fraction distribution which results in the largest second frequency ω_2 is depicted in Fig. 8b. The optimized mode is also flexural one and the corresponding frequency is $\omega_2 = 5032.9$ Hz, which is 48.1% larger than a monolithic copper beam and 13.3% larger than a monolithic tungsten beam. The optimized third frequency which corresponds to the axial mode, $\omega_3 = 6649.7$ Hz, is 51.8% and 16.9% larger than a monolithic copper and tungsten beams, respectively.

Table 2. The first three optimized frequencies (Hz) of FG beam for various boundary conditions ($p = 3$, $q = 2$).

BCs	Mode					
	1	Diff. (%)	2	Diff. (%)	3	Diff. (%)
CF	1179.3	Cu (75.0) W (34.5)	5032.9	Cu (48.1) W (13.2)	6649.7	Cu (51.8) W (16.9)
SS	2536.2	Cu (40.2) W (7.8)	7974.1	Cu (33.7) W (2.6)	12963.6	Cu (48.0) W (13.9)
CS	3635.9	Cu (43.2) W (10.0)	9115.4	Cu (37.1) W (5.1)	13135.7	Cu (47.1) W (13.2)
CC	4942.8	Cu (50.3) W (14.5)	10252.3	Cu (42.7) W (8.3)	13118.6	Cu (49.8) W (15.3)

To investigate the effect of boundary conditions on the optimized W/Cu beam, the lowest three optimized frequencies and the increase of frequencies over monolithic copper and tungsten beams are presented in Table 2 for four boundary conditions. The orders of basis function are $p = 3$ and $q = 2$ and the number of elements is 256 ($e_x = 16$, $e_z = 16$). From Table 2, some noteworthy conclusions are as follows:

a) the value of optimized frequency increases as the end boundary condition is restrained as expected,

b) the increase of frequency is the largest for CF beam, followed by CC, CS and SS beams for flexural mode, whereas its rate for SS beam is larger than that for CS beam for an axial mode,

c) the lower flexural mode exhibits larger increase of frequency than the higher flexural one.

Finally, the effect of slenderness ratio on the fundamental optimized frequency of CF beam is plotted in Fig. 9. It is seen that the slenderness ratio does not cause a significant influence on the fundamental optimized frequency.

a)

b)

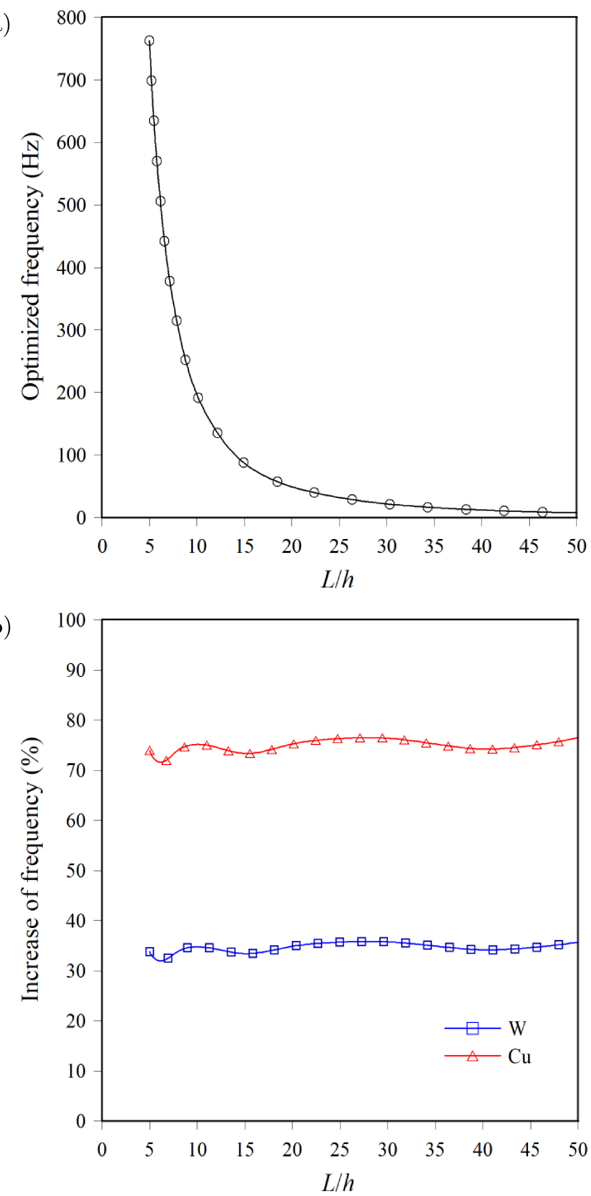

Fig. 9. Optimized and increase of frequencies for W and Cu with respect to L/h; a) optimized frequency, b) increase of frequency for W and Cu.

7. Conclusions

In this paper, an improved methodology for the simulation and optimization of the free vibrational response of W/Cu bidirectional functionally graded beams is developed. The geometric description and the displacement fields are expressed with the aid of the one-dimensional NURBS basis functions. On the other hand, the gradation of material properties is represented by two-dimensional NURBS ones. A differential evolution algorithm is used to optimize the volume fraction distribution at the control points that maximize the natural frequency. The proposed method is validated with results from other researchers and a good correlation is achieved for the bidirectional functionally graded beams tested in this study. Through numerical examples, the optimized volume fraction distribution and the effects of number of elements, boundary conditions and slenderness ratios on the optimized natural frequencies are investigated. Based on the parametric studies, the following conclusions may be drawn:

1) The computed natural frequencies and optimized natural frequencies for bidirectional functionally graded beams are found to be in good agreement with the reference results available in the literature.

2) Increase of the optimized frequency is the largest for the clamped-free beam, followed by clamped-clamped, clamped-simple and simple-simple beams for flexural mode, whereas its rate for simple-simple beam is larger than that for clamped-simple beam for an axial mode.

3) The lower flexural mode exhibits larger increase of frequency than the higher flexural one due to optimization.

4) The slenderness ratio does not cause a significant influence on the fundamental optimized frequency.

5) The present NURBS-based isogeometric analysis can be used with differential evolution in order to solve the optimization problems involving the free vibration analysis of bidirectional functionally graded beams.

Acknowledgements

This research was supported by Basic Science Research Program through the National Research Foundation of Korea (NRF) funded by the Ministry of Education (2017R1D1A1B03030412).

This is an original paper which has neither previously, nor simultaneously, in whole or in part, been submitted anywhere else.

References

1. K.K. Pradhan, S. Chakraverty, *Free vibration of Euler and Timoshenko functionally graded beams by Rayleigh–Ritz method*, Composites Part B: Engineering, **51**, 175–184, 2013.

2. P.T. Vo, H.T. Thai, T.K. Nguyen, F. Inam, J. Lee, *A quasi-3D theory for vibration and buckling of functionally graded sandwich beams*, Composite Structures, **119**, 1–12, 2015.

3. H.T. Thai, P.T. Vo, *Bending and free vibration of functionally graded beams using various higher-order shear deformation beam theories*, International Journal of Mechanical Sciences, **62**, 57–66, 2012.

4. Y. Huang, X.F. Li, *Bending and vibration of circular cylindrical beams with arbitrary radial nonhomgeneity*, International Journal of Mechanical Sciences, **52**, 595–601, 2010.

5. M. Şimşek, *Fundamental frequency analysis of functionally graded beams by using different higher-order beam theories*, Nuclear Engineering and Design, **240**, 697–705, 2010.

6. M. Aydogdu, V. Taskin, *Free vibration analysis of functionally graded beams with simply supported edges*, Materials & Design, **28**, 1651–1656, 2007.

7. D.S. Mashat, E. Carrera, A.M. Zenkour, S.A. Al Khateeb, M. Filippi, *Free vibration of FGM layered beams by various theories and finite elements*, Composites Part B: Engineering, **59**, 269–278, 2014.

8. X.F. Li, Y.A. Kang, J.X. Wu, *Exact frequency equations of free vibration of exponentially functionally graded beams*, Applied Acoustics, **74**, 413–420, 2013.

9. C. Jin, X. Wang, *Accurate free vibration analysis of Euler functionally graded beams by the weak form quadrature element method*, Composite Structures, **125**, 41–50, 2015.

10. S.A. Sina, H.M. Navazi, H. Haddadpour, *Exact frequency equations of free vibration of exponentially functionally graded beams*, Materials & Design, **30**, 741–747, 2009.

11. M. Nemat-Alla, *Reduction of thermal stresses by developing two-dimensional functionally graded materials*, International Journal of Solids and Structures, **40**, 7339–7356, 2003.

12. C.F. Lü, W.Q. Chen, R.Q. Xu, C.W. Lim, *Semi-analytical elasticity solutions for bi-directional functionally graded beams*, International Journal of Solids and Structures, **45**, 258–275, 2008.

13. L. Zhao, W.Q. Chen, C.F. Lü, *Symplectic elasticity for bi-directional functionally graded materials*, Mechanics of Materials, **54**, 32–42, 2012.

14. M. Şimşek, *Bi-directional functionally graded materials (BDFGMs) for free and forced vibration of Timoshenko beams with various boundary conditions*, Composite Structures, **133**, 968–978, 2015.

15. M. Şimşek, *Buckling of Timoshenko beams composed of two-dimensional functionally graded material (2D-FGM) having different boundary conditions*, Composite Structures, **149**, 304–314, 2016.

16. Z.H. Wang, X.H. Wang, G.D. Xu, S. Cheng, T. Zeng, *Free vibration of two-directional functionally graded beams*, Composite Structures, **135**, 191–198, 2016.

17. D. Hao, C. Wei, *Dynamic characteristics analysis of bi-directional functionally graded Timoshenko beams*, Composite Structures, **141**, 253–263, 2016.

18. A.J. Goupee, S.S. Vel, *Optimization of natural frequencies of bidirectional functionally graded beams*, Structural and Multidisciplinary Optimization, **32**, 473–484, 2006.

19. L.F. Qian, H.K. Ching, *Static and dynamic analysis of 2-D functionally graded elasticity by using meshless local Petrov-Galerkin method*, Journal of the Chinese Institute of Engineers, **27**, 491–503, 2004.

20. L.F. Qian, R.C. Batra, *Design of bidirectional functionally graded plate for optimal natural frequencies*, Journal of Sound and Vibration, **280**, 415–424, 2005.

21. C.M.C. Roque, P.A.L.S. Martins, *Differential evolution for optimization of functionally graded beams*, Composite Structures, **133**, 1191–1197, 2015.

22. C.M.C. Roque, P.A.L.S. Martins, A.J.M. Ferreira, R.M.N. Jorge, *Differential evolution for free vibration optimization of functionally graded nano beams*, Composite Structures, **156**, 29–34, 2016.

23. G.C. Tsiatas, A.E. Charalampakis, *Optimizing the natural frequencies of axially functionally graded beams and arches*, Composite Structures, **160**, 256–266, 2017.

24. T.J.R. Hughes, J.A. Cottrell, Y. Bazilevs, *Isogeometric analysis: CAD, finite elements, NURBS, exact geometry and mesh refinement*, Computer Methods in Applied Mechanics and Engineering, **194**, 4135–4195, 2005.

25. J.A. Cottrell, T.J.R. Hughes, Y. Bazilevs, *Isogeometric Analysis, Toward Integration of CAD and FEA*, Wiley, New York, 2009.

26. C. Adam, S. Bouaddallah, M. Zarroug, H. Maitournam, *Improved numerical integration for locking treatment in isogeometric structural elements, Part I: Beams*, Computer Methods in Applied Mechanics and Engineering, **279**, 1–28, 2014.

27. F. Auricchio, L. Beirão da Veiga, J. Kiendl, C. Lovadina, A. Reali, *Locking-free isogeometric collocation methods for spatial Timoshenko rods*, Computer Methods in Applied Mechanics and Engineering, **263**, 113–126, 2013.

28. R. Bouclier, T. ElGuedj, A. Combescure, *Locking free isogeometric formulations of curved thick beams*, Computer Methods in Applied Mechanics and Engineering, **245-246**, 144–162, 2012.

29. J. Kiendl, F. Auricchio, T.J.R. Hughes, A. Reali, *Single-variable formulations and isogeometric discretizations for shear deformable beams*, Computer Methods in Applied Mechanics and Engineering, **284**, 988–1004, 2015.

30. A.T. Luu, N.I. Kim, J. Lee, *NURBS-based isogeometric vibration analysis of generally laminated deep curved beams with variable curvature*, Composite Structures, **119**, 150–165, 2015.

31. H. Kapoor, R.K. Kapania, *Geometric nonlinear NURBS isogeometric finite element analysis of laminated composite plates*, Composite Structures, **94**, 3434–3447, 2012.

32. S. Shojaee, N. Valizadeh, E. Izadpanah, T. Bui, T.V. Vu, *Free vibration and bucking analysis of laminated composite plates using the NURBS-based isogeometric finite element method*, Composite Structures, **94**, 1677–1693, 2012.

33. C.H. Thai, H. Nguyen-Xuan, N. Nguyen-Thanh, T.H. Le, T. Nguyen-Thoi, T. Rabczuk, *Static, free vibration, and buckling analysis of laminated composite Reissner Mindlin plates using NURBS-based isogeometric approach*, International Journal for Numerical Methods in Engineering, **91**, 571–603, 2012.

34. Y. Bazilevs, M.C. Hsu, J. Kiendl, R. Wüchner, K.U. Bletzinger, *3D simulation of wind turbine rotors at full scale. Part II: Fluid-structure interaction modeling with composite blades*, International Journal for Numerical Methods in Fluids, **65**, 236–253, 2011.

35. D.J. Benson, Y. Bazilevs, M.C. Hsu, T.J.R. Hughes, *Isogeometric shell analysis: The Reissner-Mindlin shell*, Computer Methods in Applied Mechanics and Engineering, **199**, 276–289, 2010.

36. D.J. Benson, Y. Bazilevs, M.C. Hsu, T.J.R. Hughes, *A large deformation, rotation-free, isogeometric analysis*, Computer Methods in Applied Mechanics and Engineering, **200**, 1367–1378, 2011.

37. J. Kiendl, K.U. Bletzinger, J. Linhard, R. Wüchner, *Isogeometric shell analysis with Kirchhoff-Love elements*, Computer Methods in Applied Mechanics and Engineering, **198**, 3902–3914, 2009.

38. T. Mori, T. Tanaka, *Average stresses in matrix and average elastic energy of materials with misfitting inclusions*, Acta Metallurgica, **21**, 571–574, 1973.

39. S.H. Shen, Z.X. Wang, *Assessment of Voigt and Mori–Tanaka models for vibration analysis of functionally graded plates*, Composite Structures, **94**, 2197–2208, 2012.

40. D. Simon, *Evolutionary Optimization Algorithms*, Wiley, New Jersey, 2013.

41. A.E. Alshorbagy, M.A. Eltaher, F.F. Mahmoud, *Free vibration characteristics of a functionally graded beam by finite element method*, Applied Mathematical Modelling, **35**, 412–425, 2011.

Received February 4, 2018; revised version May 31, 2018.